

THE STRUCTURE OF HIGH STREHL RATIO POINT-SPREAD FUNCTIONS

MARSHALL D. PERRIN¹

Astronomy Department, University of California, Berkeley, CA 94720

ANAND SIVARAMAKRISHNAN AND RUSSELL B. MAKIDON

Space Telescope Science Institute, 3700 San Martin Drive, Baltimore, MD 21218

BEN R. OPPENHEIMER

Astrophysics Department, American Museum of Natural History,
Central Park West at 79th Street, New York, NY 10024

AND

JAMES R. GRAHAM

Astronomy Department, University of California, Berkeley, CA 94720

Received 2003 March 28; accepted 2003 June 20

ABSTRACT

We describe the symmetries present in the point-spread function (PSF) of an optical system either located in space or corrected by an adaptive optics (AO) system to Strehl ratios of about 70% and higher. We present a formalism for expanding the PSF to arbitrary order in terms of powers of the Fourier transform of the residual phase error over an arbitrarily shaped and apodized entrance aperture. For traditional unapodized apertures at high Strehl ratios, bright speckles pinned to the bright Airy rings are part of an antisymmetric perturbation of the perfect PSF, arising from the term that is first order in the residual phase error. There are two symmetric second-degree terms. One is negative at the center and, like the first-order term, is modulated by the perfect image's field strength—it reduces to the Maréchal approximation at the center of the PSF. The other is nonnegative everywhere, zero at the image center, and can be responsible for an extended halo—which limits the dynamic range of faint companion detection in the darkest portions of the image. In regimes where one or the other term dominates the speckles in an image, the symmetry of the dominant term can be exploited to reduce the effect of those speckles, potentially by an order of magnitude or more. We demonstrate the effects of both secondary obscuration and pupil apodization on the structure of residual speckles and discuss how these symmetries can be exploited by appropriate telescope and instrument design, observing strategies, and filter bandwidths to improve the dynamic range of high dynamic range AO and space-based observations. Finally, we show that our analysis is relevant to high dynamic range coronagraphy.

Subject headings: circumstellar matter — instrumentation: adaptive optics — methods: analytical — methods: numerical — planetary systems — techniques: image processing

1. INTRODUCTION

The direct detection of extrasolar planets, or exoplanets, has become a major astronomical and biological focus. The technical problems that must be overcome in order to image such objects near their parent stars are formidable. A Jovian planet is about a million times fainter than the star at a wavelength of $1.6 \mu\text{m}$, and a terrestrial planet is 10^9 times fainter at $0.8 \mu\text{m}$. Much effort has been expended on inventing or rediscovering shaped and apodized pupil telescopes and developing novel coronagraphic techniques to enable these detections. Many of these pioneering studies assume perfect optics, with no scattered light, no ghost images, and a perfectly corrected wave front. Here we admit the possibility of imperfectly corrected wave fronts and investigate the structure of the point-spread function (PSF) of a good but not perfect imaging system through an arbitrarily shaped and apodized pupil.

We extend earlier work by Bloemhof et al. (2001) and Sivaramakrishnan et al. (2002) to show that the PSF may be expanded in an infinite Taylor-like series, with the property that all even terms in the series are symmetric and all odd terms are antisymmetric. Thus the sum of this series, the

overall PSF, need have no particular symmetry. However, we show that for particular portions of parameter space (e.g., some telescope aperture geometry, Strehl ratio S , and angular separation from the PSF center), the sum may be dominated by one or another individual term. We identify two such regimes: very high Strehl ratio images ($S > 95\%$), which are dominated almost everywhere by the antisymmetric first-order term (as described by Bloemhof 2003), and moderate Strehl ratio images ($70\% < S < 90\%$), which are dominated by a symmetric second-order term in the image halo, particularly for apodized apertures. In these regimes, where speckle formation is dominated by a single term in the PSF expansion, there will be appreciable amounts of symmetry to the speckle patterns, which may be exploited for significant gains in signal-to-noise ratios (S/Ns) as part of the data reduction process.

We also theoretically and numerically demonstrate that apodizing the pupil reduces the effects of the first-order antisymmetric component of the aberrated PSF and allows the symmetric component to become the dominant aberration at lower Strehl ratios, as well as for a larger angular extent than in the case of a completely clear aperture. A knowledge of these PSF properties could ease the extremely stringent demands placed on the optical quality of a telescope dedicated to finding Jovian or terrestrial exoplanets.

¹ Michelson Graduate Fellow.

In general, the PSF of an adaptively corrected optical system consists of a diffraction limited core (e.g., an Airy function for a circular aperture) superposed on an extended halo composed of numerous “speckles” that result from the uncorrected components of the wave front. If we characterize atmospheric turbulence using Fried’s parameter r_0 , then there will be about $(D/r_0)^2$ speckles present in a halo of size D/r_0 , comparable to the size of the seeing disk in uncorrected images. These speckles fluctuate rapidly on a time-scale of r_0/v (where v is the wind speed), giving speckle lifetimes around a few hundredths of a second in practice.

Racine et al. (1999) first described the problem of speckle noise being the dominant noise source in high Strehl ratio AO images by considering how clumping of uncorrected light affects the S/N of aperture photometry near bright stars. Bloemhof et al. (2001) developed a first-order theory of PSF structure for symmetric, clear aperture telescopes, and Sivaramakrishnan et al. (2002) developed the complete second-order expansion of the PSF of a well-corrected image taken with an arbitrarily shaped and apodized pupil. We extend the latter work to arbitrary order and explore the nature of various terms in the infinite series expansion in order to determine how understanding the partially corrected PSF can help us design instruments to detect faint structure around stars, with photometry and spectroscopy of debris disks and exoplanets as our goal.

Bloemhof et al. (2001) showed that first-order speckles do not appear in dark areas of the underlying monochromatic perfectly corrected image, describing them as being “pinned” to the bright Airy rings on the image. They suggest a “speckle sweeping” strategy for the highest Strehl ratio images, when the first-order term is the dominant aberration. Sivaramakrishnan et al. (2002) demonstrated that these pinned speckles will still occur near the cores of images taken with arbitrarily shaped, unapodized entrance apertures and that first-order pinned speckles are part of an antisymmetric perturbation on the perfectly corrected PSF for any aperture geometry. Knowledge of this antisymmetry can be used to improve ways of obtaining and reducing high Strehl ratio imaging data. Observing strategies can be modified to exploit this phenomenon by selecting a filter band-pass that enables these pinned speckles to be seen, and therefore removed from the data, thereby increasing the dynamic range of the observations (Bloemhof 2003). In this work we show that even simple apodization of the entrance pupil suppresses the first-order speckle term in regimes accessible from either space- or ground-based telescopes.

In this paper we also examine the two second-degree terms in the expansion of the PSF: Sivaramakrishnan et al. (2002) identified one with the Maréchal approximation or the Strehl intensity (Born & Wolf 1993) and the other with an extended “second-order halo.” For a given aperture, their sizes are entirely dependent on the spatial frequencies present in the phase function. We show that one of the second-degree terms, which we call the second-order Strehl term, dominates the first-order term near the image core.

The second-order halo term sets a Strehl ratio–dependent theoretical limit on the dynamic range achievable with speckle sweeping observing strategies. This term also sets a dynamic range limit for diffraction-limited single-stage coronagraphy on future ExAO systems (which will deliver Strehl ratios of $\sim 90\%$ or higher; Makidon et al. 2003), as well as dedicated, space-based high dynamic range imaging telescopes such as Jovian or terrestrial planet-finding mis-

sions, unless multistep coronagraphic methods (Labeyrie 2003; Soummer 2002) are implemented.

2. THE FULL EXPANSION FOR THE PARTIALLY CORRECTED PSF

We briefly restate the notation of Sivaramakrishnan et al. (2002); the telescope entrance aperture and all phase effects in a monochromatic wave front impinging on the optical system are described by a real aperture illumination function $A(x, y)$ multiplied by a unit modulus function $A_\phi(x, y) = e^{i\phi(x, y)}$. Aperture plane coordinates are (x, y) in units of the wavelength of light, and image plane coordinates are (ξ, η) in radians. Deviations from a plane wave are described by a real wave front phase function ϕ that possesses a zero mean value over the aperture plane,

$$\frac{\int A\phi dx dy}{\int A dx dy} = 0. \quad (1)$$

While the choice of the phase zero point is arbitrary, selecting the wave front piston origin using equation (1) enables a clean separation between the two second-degree terms in our expansion, as we will show in § 3.3.

The perfect optical system with no phase aberration has the aperture illumination function A .

We assume that the electric field in the image plane is described by the Fourier transform (FT) of the field in the aperture plane (e.g., Goodman 1968). We write the FT of a function A as a and the FT of ϕ as Φ by changing case to indicate a transform. The aperture illumination function with phase aberrations is

$$A_{AO} = AA_\phi, \quad (2)$$

with a corresponding “amplitude-spread function” (ASF) of $a_{AO} = a \star a_\phi$ (where \star denotes the convolution operation). The ASF is proportional to the electric field in the image plane and is a complex-valued function of angular image plane coordinates (ξ, η) . The PSF of this optical system is

$$p_{AO} = a_{AO}a_{AO}^*, \quad (3)$$

(where the $*$ operator denotes the complex conjugate). At any location in the pupil plane, A_{AO} can be expanded in an absolutely convergent series in ϕ for any finite value of the phase function

$$A_{AO} = AA_\phi = A(1 + i\phi - \phi^2/2 + \dots). \quad (4)$$

We have to Fourier transform this in order to get the ASF and PSF. In order to write this economically, we define the n -fold convolution operator \star^n by, e.g., $x \star^3 y \equiv x \star y \star y \star y$. For completeness we note that $x \star^0 y \equiv x$.

Since the Fourier transform is a linear operator, we may take the transform of the series expansion of A_{AO} in equation (4) on a term-by-term basis, obtaining

$$a_{AO} = \sum_{k=0}^{\infty} \frac{i^k}{k!} (a \star^k \Phi), \quad (5)$$

which possesses a complex conjugate of

$$a_{AO}^* = \sum_{k=0}^{\infty} \frac{(-i)^k}{k!} (a^* \star^k \Phi^*). \quad (6)$$

The PSF $p_{AO} = a_{AO} a_{AO}^*$ is given by the double infinite sum

$$p_{AO} = \sum_{k=0}^{\infty} \sum_{j=0}^{\infty} \frac{i^k}{k!} (a \star^k \Phi) \frac{(-i)^j}{j!} (a^* \star^j \Phi^*).$$

We can reexpress this more usefully by grouping all terms of the same total order in Φ and Φ^* —that is, terms of constant $n = j + k$ (as in the binomial theorem),

$$p_{AO} = \sum_{n=0}^{\infty} \sum_{k=0}^n \frac{i^k (-i)^{n-k}}{k!(n-k)!} (a \star^k \Phi) (a^* \star^{n-k} \Phi^*).$$

In other words, the n th order portion of the expansion of the PSF will be given by

$$p_n = i^n \sum_{k=0}^n \frac{(-1)^{n-k}}{k!(n-k)!} (a \star^k \Phi) (a^* \star^{n-k} \Phi^*), \quad (7)$$

where we have factored out the appropriate power of i .

Since A and ϕ are real functions, a and Φ are Hermitian; i.e., their real parts are symmetric functions of their arguments, and their imaginary parts are antisymmetric functions (this, and all other Fourier results we use, can be found in Bracewell 1986). Furthermore, multiplication, addition, subtraction, and convolution of Hermitian functions produce Hermitian functions, so every component of each term in equation (7) is Hermitian.

The sum in equation (7) can further be broken into parts by grouping pairs of terms in which the power of a in one matches the power of a^* in the other. This general expansion predicts a pinned term at every order; the first and last terms in the n th order portion of the expansion (eq. [7]) contain either only a or a^* as a factor—the sum of these produces a real contribution to the PSF that is modulated by the ASF a .

2.1. Minimum Speckle Size

Since the phase function ϕ (or any power of it) never appears in the aperture illumination function in equation (4) by itself but is always multiplied by the aperture function A , we only find terms such as $A\phi$, $A\phi^2$, ... in the expansion for A_{AO} . Therefore, the FTs of these terms, $a \star \Phi$, $a \star^2 \Phi$, $a \star^3 \Phi$, ..., are the only way we find Φ in the eventual PSF. This means that all structure in the FT of the phase function ϕ is always convolved with the ASF. Even the sharpest peaks that might occur in this transform will always appear in the PSF after such convolution. Since the width of a is just the angular resolution of the telescope, the sharpest speckles in the PSF cannot be smaller than the angular resolution of the telescope. Since the expansion (4) converges absolutely, this statement's veracity does not depend of the aberration being small compared with unity; it is a general result valid for any PSF—speckles cannot be smaller than λ/D . Although there are simpler ways of demonstrating this fact, we use this argument as an exercise in tracing commonly used descriptions of optical aberrations to features in the PSF.

2.2. Symmetry of Even and Odd Terms

All terms of odd degree (i.e., p_n , with n being an odd number) will be antisymmetric with respect to the image origin. This follows by precisely the same logic originally applied to the first-order term: odd terms are given by i times the imag-

inary part of a Hermitian function, which is itself antisymmetric. Likewise, all even terms must be symmetric, because they are given by the real portions of Hermitian functions. What is potentially useful for increasing dynamic range of the direct imaging described here is the fact that under different conditions (Strehl ratio, separation from the central star, pupil geometry, and apodization), different terms dominate the speckle noise in the image. Knowledge of the expected symmetry or antisymmetry can be used in instrument design, filter specification, and data reduction to improve the S/N for the same depth of exposure.

2.3. The Effect of Scintillation

The above-derived expansion holds true for arbitrary entrance apertures A . We may model scintillation as a variation in amplitude at the telescope aperture: $A = A_{tel}[1 + \epsilon(x, y)]$, where A_{tel} is the telescope aperture function in the absence of scintillation and ϵ is a zero mean function representing the change in amplitude across that aperture due to scintillation (termed “flying shadows” by Dravins et al. 1997a). It is then seen that the same expression for the expanded PSF continues to hold, with a being replaced by $a \star (\delta + E)$ (where δ is a Dirac delta function, the FT of the constant 1, and E is the FT of ϵ). Therefore, scintillation may redistribute power in a PSF compared with the PSF without scintillation but will always affect symmetric speckles in a symmetric manner, and vice versa for antisymmetric speckles. Random changes in aperture throughput will also modify the perfect PSF (term 0), scattering some light into the dark rings of the Airy pattern; this will allow pinned speckles to begin appearing in these dark rings as well.

2.4. AO Control Radius

It is instructive to consider the idea of the AO control radius $\theta_{AO} \equiv \lambda/2d$ (where λ is the observing wavelength and d is the interactuator spacing as projected back to the primary mirror—that is, the physical actuator spacing times the magnification factor from DM to primary; here we assume that projected wave front sensor [WFS] subaperture spacing and DM actuator spacing are comparable). This is an angular distance in the image plane, resulting from the inability of the deformable mirror to compensate for wave front aberrations beyond its spatial Nyquist frequency. Correcting the wave front on spatial scales up to but not beyond the spatial frequency of $1/2d$ pulls light from an extended halo into the core of the PSF. As Strehl ratios get higher, when first the extended Maréchal [$S \sim \exp(-\sigma_\phi^2)$] and then the Maréchal ($S \sim 1 - \sigma_\phi^2$) approximations become valid, the halo outside the AO control radius θ_{AO} becomes less and less affected by improved wave front correction within the AO spatial frequency control band. When the second-order expansion of the PSF is a good representation of the PSF, correcting ϕ at a spatial frequency of $1/2d$ affects the PSF up to an angle $2\theta_{AO} = \lambda/d$ from the image center, because terms that are quadratic in the Fourier transform of the phase (Φ) contain the “doubled” spatial frequency due to the multiplication of two functions containing signal at a spatial frequency of $\lambda/2d$. By the time the second-order terms are negligible, and the first-order expansion of the PSF is applicable, correcting the wave front at scales of $1/2d$ results in improvement of the PSF only within a radius of θ_{AO} .

As a result, for Strehl ratios of about 80% or lower, the idea of an AO control radius holds in only an approximate sense, but as Strehl ratios climb into the 90% and higher range, θ_{AO} becomes a more rigorous limit on the region of the PSF that is controlled by active or adaptive optics. This is a direct reflection of the way e^x is approximated by a first-, second-, or higher order expansion in x .

It has been suggested that the performance of an AO coronagraph can be improved by using the light that would otherwise have been blocked by the image plane mask for wave front sensing. Rather than using a dichroic to split light for WFS, a mask fabricated as a hole in a mirror can be used to split the light, with the reflected portion going to the science camera and the portion that passes through the hole (the core of the Airy function) going to the WFS. The appeal of this approach is that it could greatly reduce the amount of non-common path optics between the WFS and science camera light paths.

However, the existence of the AO control radius limits the effectiveness of this approach: Passing the light through a pinhole before sensing acts as a filter limiting the spatial frequencies that reach the WFS. For reasonable spot sizes, this will limit AO performance by preventing correction of high spatial frequency aberrations. For example, a Lyot spot that is $5\lambda/D$ in diameter will pass only spatial frequencies of five cycles across the primary diameter D or lower. In this case the effective AO control radius will be set, not by the Nyquist frequency of the WFS, but by the maximum spatial frequency passed by this stop. In the case in which the same wavelength is used for science and WFS, no useful correction is possible with this approach: the effective AO control radius will equal the spot radius. Speckles outside the Lyot spot correspond to aberrations on higher spatial frequencies than reach the WFS and thus will not be corrected. If different wavelengths are used for WFS and science, then the AO control radius can be made larger than the spot diameter, but by a factor no greater than $\lambda_{sci}/\lambda_{WFS}$. This places a fundamental limit on the maximum Strehl ratio achievable with such systems, no matter how many WFS subapertures or DM actuators they may have.

However, as Macintosh et al. (2002) and Poyneer & Macintosh (2003) demonstrate, matching the hole size and geometry to that of the wave front sensors can improve AO system performance. By setting the hole to the size that corresponds to the spatial Nyquist frequency of the WFS (that is, by making the hole radius equal to the AO control radius), this approach will prevent aliasing of spatial frequencies in the WFS, by passing only those aberrations that fall within the sensing bandpass of the wave front sensing system. This will result in improved WFS performance by eliminating aliasing of uncorrectable higher spatial frequencies. However, the larger pinhole required for this approach is too large for use as a Lyot spot, so this approach will still require a beam splitter to separate light for WFS and science.

3. THE SECOND-ORDER EXPANSION FOR THE PARTIALLY CORRECTED PSF

In order to demonstrate the use of our general expansion for the PSF, we rederive the second-order expansion given by Sivaramakrishnan et al. (2002) from equation (7). This second-order truncation is valid when the largest absolute value of the phase aberration within the aperture is

significantly less than unity. Evaluating the expression in equation (7) for $n = 2$, we find that

$$p_2 = i^2 \left[\frac{1}{2!} (a \star^0 \Phi)(a^* \star^2 \Phi^*) + \frac{-1}{1!} (a \star^1 \Phi)(a^* \star^1 \Phi^*) + \frac{1}{2!} (a \star^2 \Phi)(a^* \star^0 \Phi^*) \right].$$

Combined with similar evaluations for the zeroth and first-order terms, this yields the second-order approximation to the PSF of

$$\begin{aligned} p_{AO} &= p_0 + p_1 + p_2 \\ &= aa^* - i[a(a^* \star \Phi^*) - a^*(a \star \Phi)] \\ &\quad + (a \star \Phi)(a^* \star \Phi^*) \\ &\quad - \frac{1}{2}[a(a^* \star \Phi^* \star \Phi^*) + a^*(a \star \Phi \star \Phi)], \end{aligned} \quad (8)$$

which agrees with the result found in equation (3) of Sivaramakrishnan et al. (2002). We now discuss the properties of each term in this expression.

3.1. The Perfect PSF: p_0

In the following discussion we refer to $p_0 = aa^*$ as the perfect image. For typical clear (i.e., unapodized) apertures, p_0 possesses bright and dark rings called Airy rings. Apodization generally fills the dark rings with light and results in a PSF with a greater FWHM intensity but with reduced diffracted light at large radii. Using Rayleigh's theorem, we note that

$$\int p_0 d\xi d\eta = \int A^2 dx dy = \int A_{AO} A_{AO}^* dx dy. \quad (9)$$

The physical interpretation of this is simply that whatever power enters the optical system and is not absorbed by apodization is relayed to the final perfect image. Phase aberrations contribute no power to the image; they just rearrange the distribution of light. By using the power theorem of Fourier theory, one can show that the total power from the term p_n contains a multiplicative factor of

$$i^n \sum_{k=0}^n \frac{(-1)^{n-k}}{k!(n-k)!}. \quad (10)$$

This factor is zero for all $n > 0$, since it is precisely $1/n!$ times $(1-1)^n$ (as can be seen by using the binomial theorem to expand the latter quantity). The net power contained in every term except p_0 is therefore zero.

The perfect PSF p_0 is symmetric: $p_0(\xi, \eta) = p_0(-\xi, -\eta)$. The fact that it is the power spectrum of A means that it is the FT of a symmetric, real function, specifically, the auto-correlation function of A . Therefore, it possesses a symmetric real part and a zero imaginary part, regardless of details of the aperture geometry.

3.2. Pinned Speckles: p_1

The first-order term,

$$\begin{aligned} p_1 &= -i[a(a^* \star \Phi^*) - a^*(a \star \Phi)] \\ &= 2 \operatorname{Im}\{[a(a^* \star \Phi^*)]\}, \end{aligned} \quad (11)$$

has been discussed for arbitrary aperture geometry and apodization by Sivaramakrishnan et al. (2002). It was first described as being a pinned term by Bloemhof et al. (2001). We reiterate here that this term is antisymmetric; any bright blob (due to the first-order pinned term) on a bright Airy ring must be accompanied by a corresponding dimming at the diametrically opposite point on the ring. Its antisymmetry forces p_1 to vanish at the center of the image, i.e., at the central peak of the PSF for typical apertures. This term cannot affect the Strehl ratio of the image, even though it is the dominant cause of decreased dynamic range within a few diffraction widths of the source in broadband AO imaging at high Strehl ratios (Sivaramakrishnan et al. 2003). This pinned speckle term is entirely due to the antisymmetric component of the function $A\phi$, because a purely symmetric function's Fourier transform contains no imaginary component.

3.3. The Extended Halo and the Strehl Intensity: p_2

Our choice of the phase origin that sets the aperture-weighted mean of ϕ to zero results in $a \star \Phi$ being zero at the image plane origin. (We choose our image plane origin to be the centroid of the intensity distribution, which is equivalent to a zero aperture-weighted mean slope of the wave front.) This enables a natural division of the second-order contribution into two terms with different behavior in the image plane,

$$p_2 = (a \star \Phi)(a^* \star \Phi^*) - \frac{1}{2} [a(a^* \star \Phi^* \star \Phi^*) + a^*(a \star \Phi \star \Phi)]. \quad (12)$$

The first term in the above expression is real and non-negative everywhere, as it is of the form zz^* , where z is a complex number. However, because of equation (1), it is zero at the origin (like the first-order pinned speckle term) and therefore does not affect the Strehl ratio either. It is merely the power spectrum of the real function $A\phi$, a fact that ensures its symmetry about the image origin. The slope of a Kolmogorov spectrum atmospheric phase function comes through to the image in this term to form the halo of a well-corrected stellar image outside the AO control radius $\theta_{AO} = \lambda/2d$.

This term contributes to decreased dynamic range everywhere, because it is not modulated by the Airy pattern. It is the dominant term in the extended halo, as its falloff with radial distance from the core of the PSF is set solely by the spatial frequencies present in the phase function. It will place second-order speckles in the dark Airy rings of a monochromatic PSF and will therefore set the ultimate limits on the dynamic range of any observational speckle sweeping techniques. We denote this term by $p_{2, \text{halo}}$.

The perfect PSF taken together with the *second* second-degree term is the Strehl intensity (Born & Wolf 1993). Like the first-order term p_1 , this term is pinned to the bright Airy rings, because it is also modulated by the size of the ASF. Combining this with the fact that it is a second-degree term suggests that it is probably not significant outside the first few Airy rings. This term is also symmetric, because it is the real part of a Hermitian function (so the entire second-degree contribution to the PSF is symmetric). At the image center it reduces the perfect PSF by $a(0)$ multiplied by the value of $(a \star \Phi \star \Phi)$ at the origin. The former quantity is $\int A dx dy$; the latter is $\int A\phi^2 dx dy$. For a clear aperture with

area A this is merely $A^2\sigma_\phi^2$, which is the well-known Maréchal approximation relating the Strehl ratio S to the variance of the phase over the aperture σ_ϕ^2 at high Strehl ratios $S = \exp(-\sigma_\phi^2) \sim 1 - \sigma_\phi^2$. For apodized apertures this yields a modified form of the Maréchal approximation, since the phase variance is weighted by the apodization. We denote this term by $p_{2, \text{Strehl}}$.

As mentioned in § 2, choosing the phase origin to ensure that the mean of the phase (weighted by the aperture throughput) is zero (eq. [1]) enables the different natures of the two contributions to the second-degree term in the partially corrected AO PSF to be easily distinguished.

3.4. A Numerical Example

Figure 1 shows a 94% Strehl ratio PSF and its first- and second-order terms. The top left frame shows the numerical monochromatic PSF p (with a logarithmic stretch) of a simulated image formed by a circular, unobstructed aperture on a twice Nyquist-sampled pixel scale. Tip-tilt errors were removed by ensuring zero mean X and Y tilts of the incoming phase screen over the aperture, so the image center is known a priori. The top middle frame shows the numerical PSF with the perfect PSF subtracted from it, $(p - p_0)$, on a linear stretch. The top right frame shows the first-order pinned speckle term p_1 with the same stretch as the top middle frame. The similarity between p_1 and $(p - p_0)$ is obvious in the inner two Airy rings of these two frames.

The antisymmetry of p_1 is also apparent in this frame. The total intensity in this frame is zero. The bottom left frame shows the second-order halo term $p_{2, \text{halo}}$ (on a linear stretch symmetric about zero, with black being assigned to the minimum value of the $p_{2, \text{Strehl}}$ term -0.06 , which occurs at the image center). Its intensity is nonnegative everywhere and zero at the image center. The bottom middle frame shows the pinned, second-degree term $p_{2, \text{Strehl}}$ (on the same stretch as the $p_{2, \text{halo}}$ frame). It is negative at the center and is the only term in the second-degree expansion of the PSF that reduces the Strehl ratio. As noted above, this term, taken together with the perfect PSF (i.e., $p_0 + p_{2, \text{Strehl}}$) is called the Strehl intensity (Born & Wolf 1993). The expression $p_0 + p_{2, \text{Strehl}}$ reproduces the Maréchal approximation of classical optics theory for the image intensity at its center at high Strehl ratios. It contains the perfect “amplitude spread function” (the image field strength) as a factor, so $p_{2, \text{Strehl}}$ could decay more rapidly with distance from the image center than the halo term $p_{2, \text{halo}}$ in ground-based AO images, depending on the power spectrum of the phase aberration and pupil apodization. The bottom right frame shows the sum of both second-degree terms (on the same stretch as each second-degree term's images).

4. NUMERICAL EXPLORATION OF SPECKLE SYMMETRY MAGNITUDES

The relative magnitude of each term in the series expansion of the PSF depends on Strehl ratio, aperture shape, and aperture apodization. In this section we present examples of the behavior and relative sizes of some of the lower order terms. We simulated AO-corrected PSFs from four circular aperture types: circular apertures with and without central obscurations, and clear and apodized apertures. For each of four different aperture types (all based on the 3.6 m AEOS telescope on Mt. Haleakula) we ran a set of simulations,

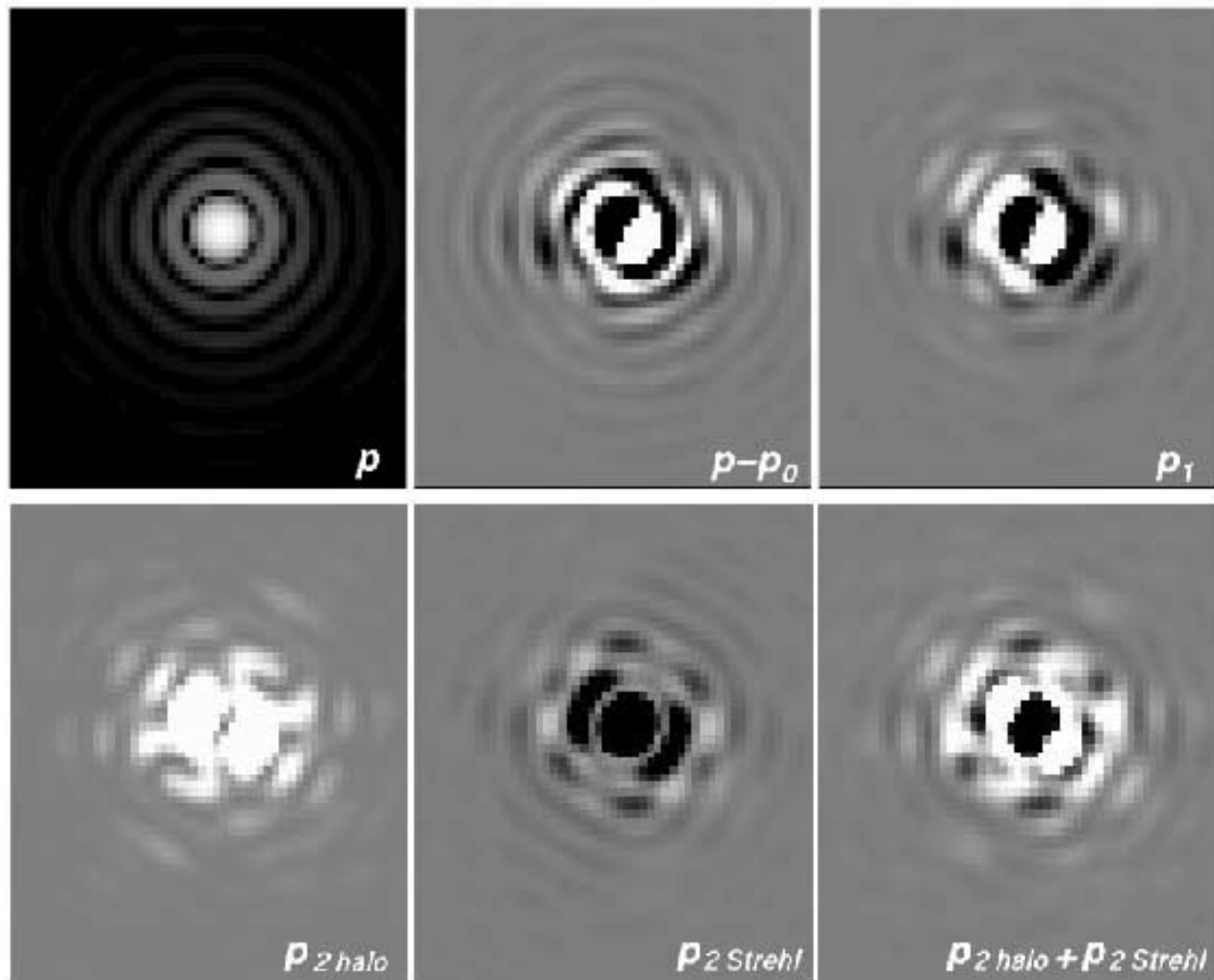


FIG. 1.—Shows that a 94% Strehl ratio PSF p , formed by a circular aperture, can be decomposed into individual terms in the power series in the Fourier transform of the phase over the aperture. The antisymmetry of the first-order term p_1 and the symmetry of the second-order terms are apparent. The positive halo term $p_{2, \text{halo}}$ is zero at the image center, as is the pinned first-order term p_1 . At these Strehl ratios the image degradation is dominated by the pinned second-order term $p_{2, \text{Strehl}}$ (see text for details).

varying the number of AO actuators from 10 to 110 across the primary, which resulted in Strehl ratios ranging from 50% to 98%.

For each simulation we generated realizations of Kolmogorov spectrum turbulence phase screens and, following the methods described in Sivaramakrishnan et al. (2001), smoothed the phase screens with a high-pass parabolic filter to mimic the action of an AO system, viz., a parabolic filter in spatial frequency space up to a Nyquist spatial frequency corresponding to the number of actuators across the pupil. This simple model of AO has been validated with fits to 70% Strehl ratio K -band data from the Palomar AO system (Oppenheimer et al. 2000) and 20% Strehl data from the 3.6 m AEOS telescope (Makidon et al. 2003). Scintillation effects (amplitude fluctuations across the pupil) have not been taken into account here, but simple calculations following the approach of Angel (1994) indicate these might reduce our calculated Strehl ratio by about 5%–10% in the H band. We reiterate the point of § 2.3 that scintillation will effect symmetric speckles in a symmetric manner, and so we do not expect it to substantially change our con-

clusions here. (See also Dravins et al. 1997b, 1998 for additional discussion of the effects of scintillation.)

We calculated the PSF of this partially corrected wave in a perfect imaging system by the methods of Fourier optics, using image plane pixels of angular size $\lambda/8D$ in order to resolve speckles clearly. We used an input pupil 128 pixels across, in a zero-filled array 1024 pixels on a side, thus ensuring fine sampling in our monochromatic image. We also calculated each term in the full expansion out to fourth-order explicitly from the input phase screens and their transforms. The Strehl ratio of the image in Figure 1 is 94%.

Before creating the image from the input phase screen, we subtracted off the mean tilt of the phase function over the clear aperture. Even though the first-order term would still retain all the properties predicted by our theory, we felt that a large tip-tilt error obscured the more interesting higher spatial frequency wave front aberrations that are found a few diffraction widths from the core of the image.

Here we describe some general properties of the results and show representative plots of 85% Strehl ratio images.

4.1. Unapodized Apertures

At the currently achievable Strehl ratio of 60%, the second-order Strehl term is the dominant perturbation to the perfect PSF p_0 on the central Airy peak, while the first-order term is most important on the first one or two Airy rings. Outside this, the second-order halo term that is largest is magnitude. Palomar and Lick observations with Strehl ratios around 60% often show a three-lobed pattern of pinned speckles on the first Airy ring (Bloemhof et al. 2001; Lloyd 2002), which may be due to the dominance of the first-order term there.

By a Strehl of 80%, the first-order term dominates on the inner three or four Airy rings, while the second-order halo term is responsible for most of the speckle power outside of the eighth Airy ring; the first- and third-order terms are down by a factor of a few relative to the symmetric second-order halo term (see Fig. 2). In this regime data reduction techniques that take advantage of the symmetry of the halo speckles may prove useful.

At Strehls above 90%, the second-order term decreases in magnitude significantly as more power moves into the diffraction limited core and does not dominate until 15 or more Airy rings out. In this regime, data reduction techniques exploiting the antisymmetry of the first-order term should be useful for the inner core of the image. This effect is more pronounced in an apodized pupil, as we discuss in § 4.2.

As Strehl ratios rise above about 98%, the first-order term increasingly dominates throughout the entire PSF outside the core.

The presence of a secondary obscuration transfers some power from the core of the unobscured aperture PSF out to the secondary's Airy rings. It therefore similarly transfers power into the pinned first-order term, resulting in a larger magnitude for this term in the outer portions of the PSF, making it closer in importance to $p_{2, \text{Strehl}}$ in the halo, as shown in Figure 2. This reduces the dominance of the symmetry in that region and will therefore lower the effectiveness of speckle symmetry subtraction for S/N gain compared with unobscured apertures.

4.2. Apodized Apertures

The idea of telescope apodization has been explored in several studies (e.g., Black 1980; Watson et al. 1991; Nisenson & Papaliolios 2001; Aime, Soummer, & Ferrari 2002; Soummer, Aime, & Falloon 2003). These pioneering efforts focused on how apodization affects PSFs of perfect or near-perfect optical systems. Nisenson & Papaliolios (2001) studied the effectiveness of apodized square apertures for detection of Earth-like planets from space, arguing that apodized square apertures had superior performance to circular apertures along certain position angles. Aime et al. (2002) and Soummer et al. (2003) derived optimized apodizations for circular aperture telescopes equipped with

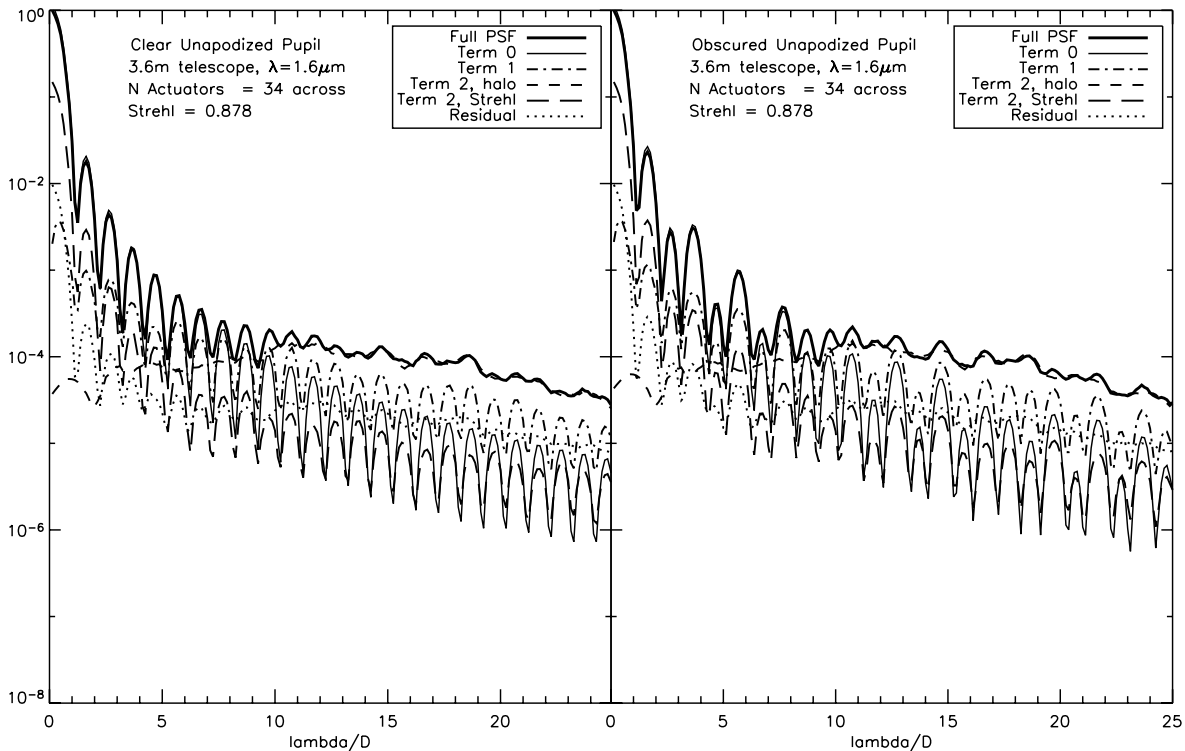


FIG. 2.—Radial profiles of the absolute value of the first few terms in the expansion of the PSF in terms of the Fourier transform of the phase over the aperture, as well as the total resulting PSF, and the residual (that is, the sum of terms 3 through infinity), in simulations of the 941 actuator AO system of the AEOS telescope on Haleakala. We plot the absolute value rather than average because the annular mean of the first-order antisymmetric term is identically zero everywhere. The left-hand panel shows results for an unobscured aperture. Outside of about $10 \lambda/D$ the second-order halo term is clearly the dominant term by about an order of magnitude above both the first-order term and the residual term (which itself is primarily due to the third- and fourth-order halo-like terms at this Strehl ratio). A secondary obscuration puts more power into the odd Airy rings, increasing the pinned first-order term for those rings (*right-hand panel*). This secondary obstruction decreases the separation between the first and second-order terms and will reduce the effectiveness of speckle symmetry techniques for noise reduction.

Lyot coronagraphs, which they conclude are preferable to square apertures for high dynamic range imaging. Here we inspect the role apodization plays in speckle suppression at high Strehl ratios.

Apodization reduces the wings of the perfect unobscured aperture PSF, so all pinned speckle terms also decrease in size. This causes the second-order halo term to become dominant at a lower Strehl ratio than on a comparable unapodized telescope. Apodization is therefore beneficial not just on telescopes with perfect optics but on real optical systems as well. This has been known informally for several years (C. Ftaclas 1997, private communication). Breckinridge & Oppenheimer (2003) point out that polarization effects from thin reflective films produce a slight natural apodization (of order a few percent) in all concave telescope mirrors, even those that are not intentionally apodized. We look at residual speckle structure in high Strehl images on pupils with a simple linear apodization (transmission changes linearly from 0 at pupil edges to 1 at its center; in order to demonstrate speckle suppression caused by simple linear apodization. Antisymmetric pinned speckles are the dominant noise source on a 98% Strehl image on clear apertures (see § 4.1). On a circular apodized pupil we find that between Strehl ratios of 80% and 97% the symmetric second-order $p_{2, \text{halo}}$ term is the dominant term by a factor of around 10 outside the first few Airy rings (Fig. 3). This suggests that Lyot coronagraphs on such pupils would exhibit significant speckle symmetry. When Strehl ratios rise past about 97% the pinned antisymmetric first-order term p_1 starts to dominate larger and larger areas around the image core. Thus for terrestrial planet finding from space the linear

pinned speckle term is probably the dominant cause of speckle noise. As Bloemhof (2003) suggests, observing strategies dedicated to utilizing this property can be used under such conditions. However, for ExAO applications from ground-based telescopes, apodized pupils can be beneficial even in the 75%–95% Strehl ratio regime.

4.3. Implications for Coronagraphy

We simulated a coronagraphic image using five independent realizations of a Kolmogorov spectrum phase screen incident of the aperture of an 8 m class telescope and a Fried length $r_0 = 80$ cm at the center of the H band. We model the effect of a 4000 actuator AO system with 64 actuators across the aperture on these phase screens and use a hard-edged coronagraphic occulting spot $4\lambda/D$ in diameter with a matched, optimized Lyot pupil stop chosen in the manner described in Sivaramakrishnan et al. (2001). We did not include scintillation effects, image placement error on the stop, or scatter from mirror imperfections or dust in our simulation. The simulated AO system produces a Strehl ratio of 98% (i.e., the phase aberration alone is responsible for a 2% Strehl hit). Other sources of scattered light will further degrade the Strehl ratio. Figure 4 shows that at higher Strehl ratios, an understanding of image symmetry properties can improve coronagraphic design, use, and data reduction methods. The benefits of this understanding increase as the Strehl ratio increases, especially in space-based imaging on very stable telescopes.

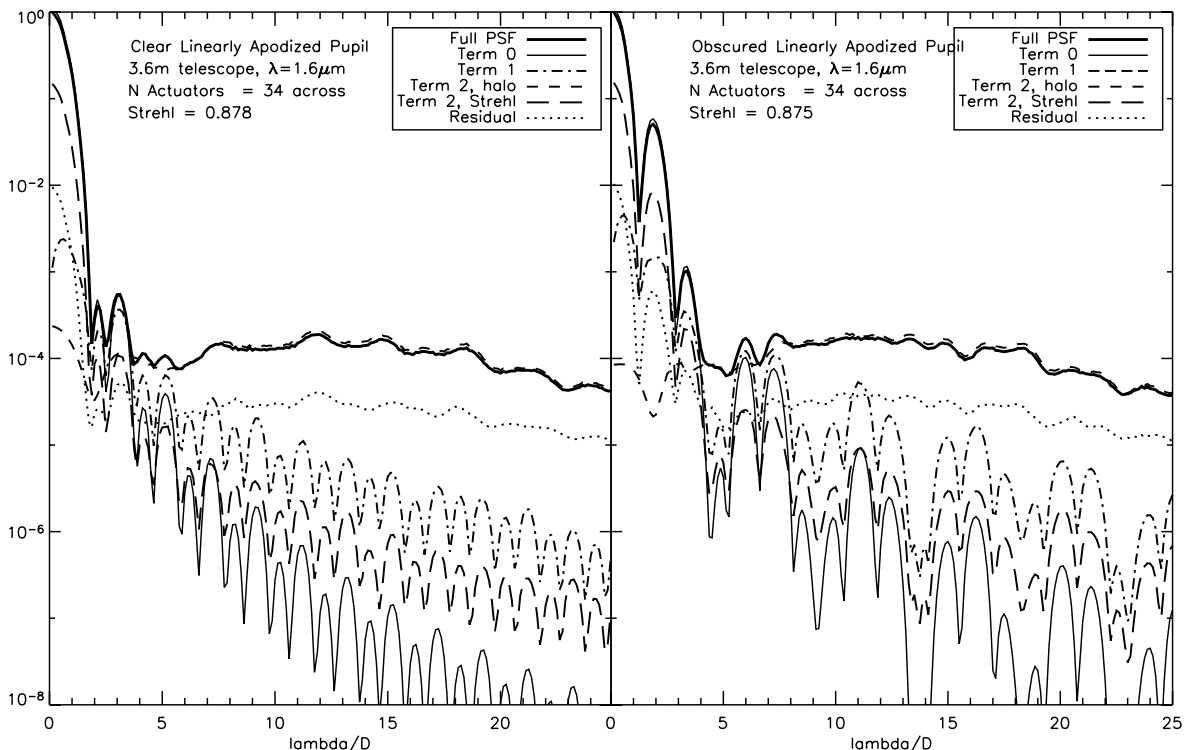


FIG. 3.—Identical to Fig. 2, except a “simplest possible” apodization has been applied to the primary; throughput changes linearly from 0 at the edges of the aperture to 1 at the center. No attempt has been made to optimize this apodization, and it is expected that more sophisticated apodizations will result in better performance. However, even this simplistic technique dramatically reduces the perfect PSF and first-order term, while the second-order halo is affected very little. If speckle symmetries are exploited to subtract off this term, the overall image halo will be reduced by nearly an order of magnitude.

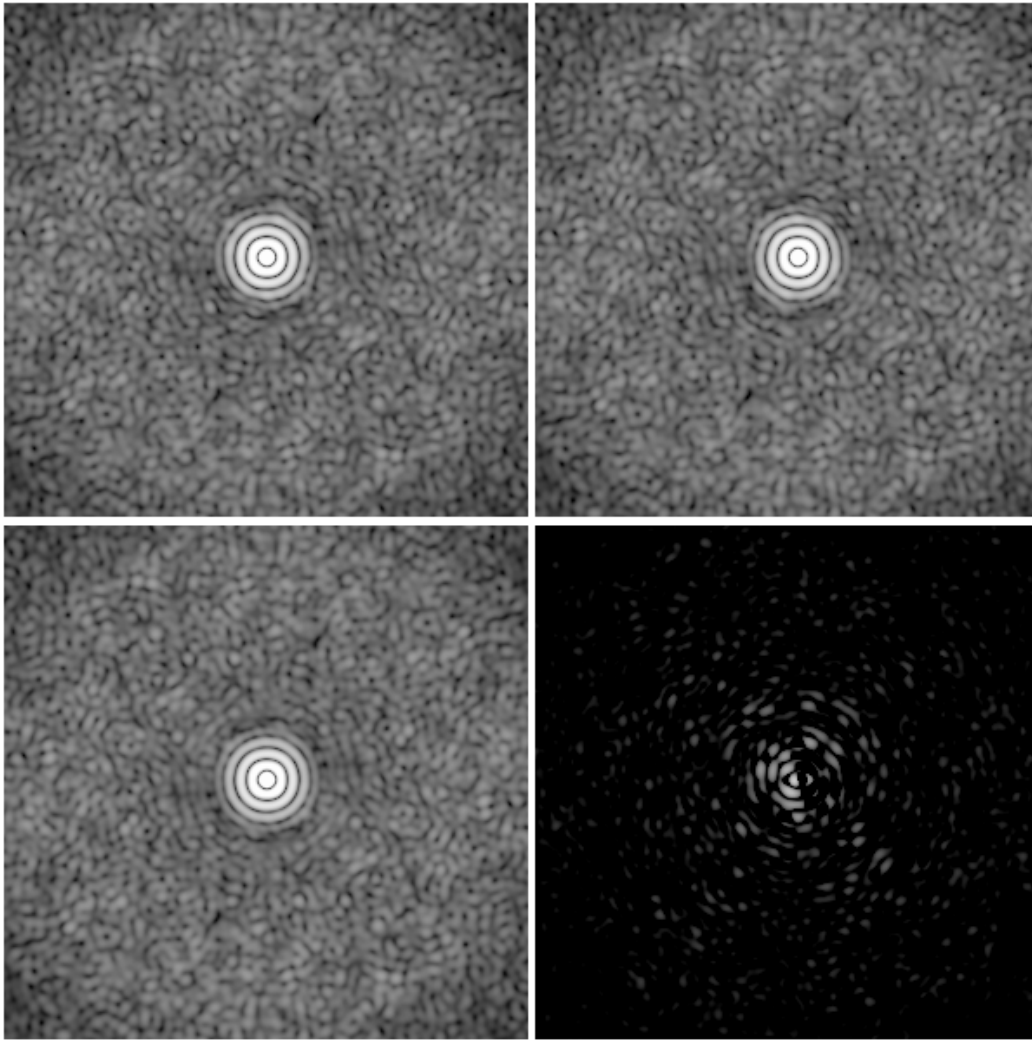


FIG. 4.—*Top left*: Shows a simulated short exposure monochromatic coronagraphic image from an 8 m telescope at the central wavelength of the H band. Co-added PSFs from five independent realizations of Kolmogorov spectrum phase screens, with $r_0 = 80$ cm are shown. The simulated AO system extrapolates Palomar AO performance to a 4000 actuators (71 across the primary) on Subaru, following Sivaramakrishnan et al. (2001). Scintillation has not been modeled explicitly. The Strehl ratio of the direct image is 98%; 97.6% of the incoming intensity has been blocked by an optimized Lyot coronagraph with an image plane stop diameter of $4\lambda/D$ radians. All four panels are on the same logarithmic scale. *Top right*: Top left image rotated by 180° about its center. *Bottom left*: Symmetric component of the original PSF, viz., half the sum of the original image and the rotated image. *Bottom right*: Absolute value of the antisymmetric component of the PSF, which is half the difference between the original image and the rotated image. A close inspection of this frame shows that much of the antisymmetric component of the speckle is generated by the presence of the secondary obscuration (which we modeled as being approximately 15% of the primary diameter).

4.4. Obscured Apertures

If even a small secondary obstruction is present, the pinned terms (p_1 and $p_{2,\text{Strehl}}$) will not die off as quickly as the corresponding term for an unobstructed aperture. This consideration could be relevant in methane-on and methane-off bands around $1.6 \mu\text{m}$, for example, since their fractional bandpasses (about $1/20$) produce visible Airy rings out to several λ/D . This argument adds weight to those presented in Tokunaga et al. (2003) for the off-axis design of a dedicated ExAO telescope.

An inspection of the antisymmetric component of the simulated 8 m ExAO coronagraphic image in the bottom right-hand panel of Figure 4 reveals the fact that the dominant cause of speckles within the first few Airy rings in this image is the increased Airy ring intensity due to the presence of a small secondary obstruction. Coronagraphic

performance on ground-based ExAO systems is therefore significantly reduced by even small secondary obstructions.

5. DISCUSSION

The expressions derived for the expansion of the point-spread function are fully general for any telescope aperture and wave front phase. However, our statements as to which term of that expansion dominates under given conditions are fundamentally statistical in nature, contingent on the assumption of Kolmogorov turbulence, which is spatially filtered by an adaptive optics system as described above. The presence of non-Kolmogorov atmospheric disturbances, or of static errors in the telescope or instrumental optical system, may change the relative importance of the various terms. In particular, further work is necessary to

ascertain the magnitude of the symmetric halo term for space-based telescopes that may possess an entirely different power spectrum of wave front errors.

Nonetheless, our theoretical and numerical results have a direct bearing on current ExAO coronagraphs under construction: the Lyot Project coronagraph on the 941 channel AO system on the 3.6 m AEOS telescope is due for first light in late 2003 (Oppenheimer, Sivaramakrishnan, & Makidon 2003); and XAOPI, a coronagraph on an 8–10 m class telescope (Macintosh et al. 2002), is projected to begin observations in 2007. Strehl ratios of 85%–95% at a wavelength of 1.65 μm are predicted for these imagers (Macintosh et al. 2002; Makidon et al. 2003). AEOS and Keck noncoronagraphic infrared data taken recently will be analyzed for the presence of features whose existence we have predicted.

By extending the second-order expansion of Sivaramakrishnan et al. (2002) to higher orders and computing individual terms for typical realizations of AO-corrected atmospheric phase aberrations, we have shown when the second-order theory is applicable. We also explain how apodization of the entrance aperture makes a difference to achievable dynamic range when the images are not perfect. Recent work (Soummer et al. 2003) has shown that optimally apodized aperture coronagraphs are more efficient than classical Lyot coronagraphs at suppressing the light from perfectly corrected stellar wave front; our analysis demonstrates ways of determining when such apodization will help increase dynamic range with instruments that are currently in use or are under construction at the moment. Our work can also be applied to coronagraphic imaging to gain theoretical insight into the sensitivity of different coronagraphic designs to residual wave front aberrations. Such understanding can affect the design of space-based telescopes dedicated to discovering Jovian and terrestrial exoplanets.

Our analysis of the properties of the partially corrected image might change the way the search space of AO observations is modeled, thereby changing survey strategies and telescope and AO system design. Clearly, the fractional filter bandwidth will limit the number of dark rings visible in an image. The presence of a secondary obstruction will also affect the dynamic range available to AO systems because of the more complex distribution of dark rings and the slower drop-off of the perfect PSF with radius, so first-order speckles will affect a larger area than in a system with an unobstructed pupil. However, at Strehl ratios of 85% and above, pupil apodization can improve dynamic range significantly close to the on-axis object.

When reducing data, the antisymmetry of the first-order speckles is prior information that should be fed into deconvolution approaches. Farther out from the center of the image, if the symmetric halo dominates noise, a different data reduction strategy is recommended. Aperture apodization and the shape of the power spectrum of the aberration affects where such a transition occurs in the image plane. The perfect PSF can also be folded into the deconvolution, because the integrated power from any individual term in our expansion is zero: each term merely redistributes power

within the image. Depending on observing conditions and instrument performance, a knowledge of the properties of the partially corrected PSF can be used to improve the detectability of faint structure near bright targets.

In the case in which a particular symmetry dominates the speckle pattern, the signal-to-noise ratio may be substantially improved by combining the image with a 180° rotated version of itself. This is essentially a variation on the PSF subtraction technique, in which the star serves as its own PSF reference when suitably rotated. This avoids the complications inherent in using a different star as a PSF reference, at the cost of reducing the overall spatial information available. This cost is not expected to be problematic for detection of point sources, although it may limit the applicability of this technique for the study of extended sources such as circumstellar disks.

In ground-based ExAO applications, our analysis is relevant to the choice of filter bandwidth. Our results can also be used to optimize the length of rapid exposures in methods that ultimately trace their origins to the dark speckle method (Labeyrie 1995). Larger filter bandwidth smears speckle out radially, and a longer exposure places more independent speckles all over the image. Both these effects cover the image with more uncorrected light. Optimized dark speckle techniques must balance detector read noise considerations against photon statistics, speckle dwell times, and the effect of a finite filter bandpass (e.g., Boccaletti, Moutou, & Abe 2000).

The PSF properties we describe here will be even more useful for long exposures on stable, space-based telescopes, since in that case speckles are extremely long-lived. A knowledge of expected speckle symmetries can be combined with the spectral approach of Sparks & Ford (2002) to improve the dynamic range limits derived in that work. An understanding of the theory presented here can yield improved instrument and detector design, observing strategies, and data reduction methods in both space- and ground-based high dynamic range astronomy, which could lead to reducing the stringency of the specifications of the optical quality of a terrestrial or Jovian planet-finding telescope.

We are grateful to E. R. Scheinerman for the elegant proof that the expression (10) is zero. We also wish to thank the Space Telescope Science Institute's Research Programs Office, Visitor Program, and Director's Discretionary Research Fund for support, as well as the American Museum of Natural History for its hospitality. This work has been supported by the National Science Foundation Science and Technology Center for Adaptive Optics, managed by the University of California at Santa Cruz under cooperative agreement AST-9876783, and is also based on work supported by the National Science Foundation under grant AST-0215793. M. P. is supported by a NASA Michelson Graduate Fellowship, under contract to the Jet Propulsion Laboratory (JPL) funded by NASA. The JPL is managed for NASA by the California Institute of Technology.

REFERENCES

- Aime, C., Soummer, R., & Ferrari, A. 2002, *A&A*, 389, 334
 Angel, J. R. P. 1994, *Nature*, 368, 203
 Black, D. C. 1980, *Project Orion: A Design Study of a System for Detecting Extrasolar Planets* (Washington, D.C.: NASA)
 Bloemhof, E. E. 2003, *ApJ*, 582, L59
 Bloemhof, E. E., Dekany, R. G., Troy, M., & Oppenheimer, B. R. 2001, *ApJ*, 558, L71
 Boccaletti, A., Moutou, C., & Abe, L. 2000, *A&AS*, 141, 157
 Born, M., & Wolf, E. 1993, *Principles of Optics* (6th ed.; Cambridge: Cambridge Univ. Press)

- Bracewell, R. N. 1986, *The Fourier Transform and its Applications* (London: McGraw Hill)
- Breckinridge, J. B., & Oppenheimer, B. R. 2003, *ApJ*, submitted
- Dravins, D., Lindegren, L., Mezey, E., & Young, A. T. 1997a, *PASP*, 109, 173
- . 1997b, *PASP*, 109, 725
- . 1998, *PASP*, 110, 610
- Goodman, J. W. 1968, *Introduction to Fourier Optics* (New York: McGraw Hill)
- Labeyrie, A. 1995, *A&A*, 298, 544
- . 2003, in *EAS Publ. Ser., Astronomy with High Contrast Imaging*, ed. C. Aime & R. Soummer, in press
- Lloyd, J. P. 2002, Ph.D. thesis, Univ. California, Berkeley
- Macintosh, B., et al. 2002, *AAS Meeting*, 201, 2101
- Makidon, R. B., Sivaramakrishnan, A., Roberts, L. C., Jr., Oppenheimer, B. R., & Graham, J. R. 2003, *Proc. SPIE*, 4860, 315
- Nisenson, P., & Papaliolios, C. 2001, *ApJ*, 548, L201
- Oppenheimer, B. R., Dekany, R. G., Hayward, T. L., Brandl, B., Troy, M., & Bloemhof, E. E. 2000, in *Proc. SPIE* 4007, 899
- Oppenheimer, B. R., Sivaramakrishnan, A., & Makidon, R. B. 2003, in *The Future of Small Telescopes* (Dordrecht: Kluwer)
- Poyneer, L., & Macintosh, B. 2003, *J. Opt. Soc. Am. A*, in press
- Racine, R., Walker, G. A. H., Nadeau, D., Doyon, R., & Marois, C. 1999, *PASP*, 111, 587
- Sivaramakrishnan, A., Hodge, P. E., Makidon, R. B., Perrin, M. D., Lloyd, J. P., Bloemhof, E. E., & Oppenheimer, B. R. 2003, *Proc. SPIE* 4860, 161
- Sivaramakrishnan, A., Koresko, C. D., Makidon, R. B., Berkefeld, T., & Kuchner, M. J. 2001, *ApJ*, 552, 397
- Sivaramakrishnan, A., Lloyd, J. P., Hodge, P. E., & Macintosh, B. A. 2002, *ApJ*, 581, L59
- Soummer, R. 2002, Ph.D. thesis, Univ. Nice, France
- Soummer, R., Aime, C., & Falloon, P. E. 2003, *A&AS*, 397, 1161
- Sparks, W., & Ford, H. C. 2002, *ApJ*, 578, 543
- Tokunaga, A. T., Ftaclas, C., Kuhn, J. R., & Baudoz, P. 2003, in *IAU Symp. 211, Brown Dwarfs*, ed. E. Martin (San Francisco: ASP), 487
- Watson, S. M., Mills, J. P., Gaiser, S. L., & Diner, D. J. 1991, *Appl. Opt.*, 30, 3253